Three-Dimensional Mathematical Model of Bio-Mechanical System: Human- Mechanized Hand Tool in Accordance to ISO 10068 Standard on the Example of Impact Drill

Wojciech RUKAT

Poznan University of Technology, Faculty of Mechanical Engineering and Management, Piotrowo 3 St, 60-965 Poznan, wojciech.rukat@put.poznan.pl

Abstract

This paper presents the development of a mathematical model of a bio-mechanical system: human – power tool, on the example of an impact drill. The physical model of the operator's upper limb with 5 degrees of freedom, in accordance with ISO 10068 standard was used. The paper presents the results of theoretical analysis regarding elementary and net displacements for individual directions. Moreover mathematical relationships describing them were determined. The result of the synthesis of these relations and the adopted (in accordance with the standard) physical model of the upper limb is the general matrix form of differential equations of motion of the analysed bio-mechanical system, built using the Lagrange's equations of the second kind.

Keywords: local vibration, mathematical model, impact drill, ISO 10068, Lagrange'a equation second kind

1. Introduction

Modelling, simulations and numerical experiments have become one of the most common tools used in the engineering practice. They cover a wide range of issues, including static calculations of elements and structures of various types [1-9], heat and/or working medium (liquids) flows [10-16], changes in the intensity of vector fields (electric and electromagnetic) [17-24] as well as vibration and dynamic analyses of constructions [25-34]. Regardless of the type of analysis conducted, energy methods, such as the finite element method (FEM) and less often the boundary element method (BEM), are used to meet the mentioned goals.

Computation of a complex system, e.g. mechanical construction, is generally limited to solving the differential equation of motion - in the case of dynamic analysis, or the equation of displacement of the system - in the case of static analysis. The generalized equation of motion in the matrix notation is presented below.

$$[M][\ddot{q}_{(t)}] + [C][\dot{q}_{(t)}] + [K][q_{(t)}] = [F_{(t)}] \tag{1}$$

where: $[M]$, $[C]$, $[K]$ are matrices of inertia, damping and elasticity,
$[F_{(t)}]$ is a vector of forces,
$[q_{(t)}]$, $[\dot{q}_{(t)}]$, $[\ddot{q}_{(t)}]$ are vectors of displacement, velocity and acceleration.

The issues of vibration impact on the human body, including the methodology of performing measurements of local vibrations, are discussed in EN ISO 5349–1 [35] and EN ISO 5349–2 [36] standards. The issue of practical way of measuring vibration of specific body parts (elbow, shoulder, etc.) has been discussed many times, among others in the works of Bąk and Cukierman-Rakoczy as well as Mrukwa, Świder and Staniek [37, 38]. Doubts regarding unambiguousness of the results obtained (vibrations of soft and hard tissues) and limitations of ethical nature (permanent fixation of the measuring equipment with a human body) have led to the creation of a unified physical model of the upper limb. The first attempts have been made in the 1980s. Possible variants of the human body modelling were presented by Książek as well as Nader and Korzeb [39, 40]. The final result of this work is the ISO 10068:1998 standard [41], which has been successfully used so far. The bio-mechanical system is the result of the synthesis of a mechanical system interpreted as the source of vibrations - e.g. a power tool with the operator's body. In this work, author has analysed and mathematically described vibrations of the bio-mechanical system for three directions of the Cartesian coordinate system, with an assumption that the device (the source of vibrations) can move in all six degrees of freedom.

The mathematical model allowed the author to analyse vibrations of individual human body parts, structural energy flow [42]. This is important when determining the permissible time of exposure to harmful factors that undoubtedly occur during the operation of a device of this type [44-46] and the implementation of occupational safety and health policy.

The aim of the work was to build a mathematical model of the bio-mechanical system: operator – power tool, basing on ISO 10068, using equivalent model of upper limb with 5-dof (degrees of freedom) , while assuming that movement of the source of vibrations in all six degrees of freedom is possible. The same physical model was used for each upper limbs. The structure of the physical model is the same for each of the direction of the coordinate system.

2. Research methodology

The basis for the carried out analysis is the 5-dof equivalent model of the upper limb, which is shown in the Figure 1. The figure presents a combined system of mass elements parallel connected in series and in parallel that represent fragments of the upper limb. Mass elements are connected with each other by both elastic and damping elements. The model also highlights the reference directions of individual coordinate axes in relation to the hand – tool handle system. The structure of the upper limb model is the same for both limbs and in all directions of the coordinate system.

The analysed device is Hitachi DH 22 PH rotary hammer, with a power of 620 W. The maximum spindle speed of this device (without load) equals 1400 rpm. In the impact drilling mode, the mechanism generates 5600 impacts per minute, each with an energy of 1.7 J. Visual inspection and analysis of the device's kinematic and assembly diagrams allow to state that the device's centre of gravity is shifted relative to the plane of the device’s body. It also does not coincide with any of handles or the spindle axis. The analysed device was presented on the figure 1.

In the presented model the device's handles are the sources of vibrations. Previous research carried out by the author showed that the device's handles vibrate in all 3 directions. The vibrations have different values for each direction, which makes it possible to suspect that the device moves in all six degrees of freedom during operation [45, 46].

Figure 1. Analysed impact drill - Hitachi DH 22 PH [own photo]

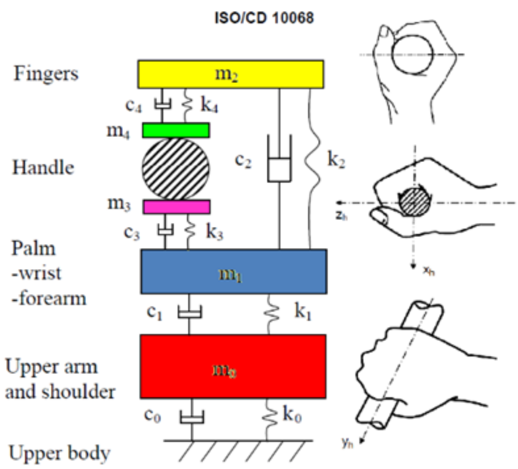

where:
m_0, m_1, m_2, m_3, m_4 - equivalent mass coefficients;
k_0, k_1, k_2, k_3, k_4 - equivalent d stiffness coefficients;
c_0, c_1, c_2, c_3, c_4 - equivalent damping coefficients

Figure 2. 5-dof equivalent model of upper limb [41]

The result of the synthesis of the considered device and the equivalent model of the upper limbs in the base direction (Z axis of the device – spindle's axis) is shown in Figure 3. Furthermore, Figure 4 shows the displacement field corresponding to the equivalent physical model of the entire bio-mechanical system (Figure 3). Figure 4 shows the linear displacement caused by one vector component of the eigenvector of the system and the angular displacement which generates the corresponding linear displacement of the device's handle. The geometric dimensions describing distances between reference points (reduction point) associated with the device handles and the centre of mass are also shown in the figure.

Figure 5 (accordingly to Figure 3) presents the equivalent model of the bio-mechanical system in the Y direction (horizontal, transverse to the spindle axis). Figure 6 shows the displacement field of the device handle on the XZ plane. The equivalent model of the system in the Y axis (vertical direction) and the associated with it displacement field are shown in Figures 7 and 8.

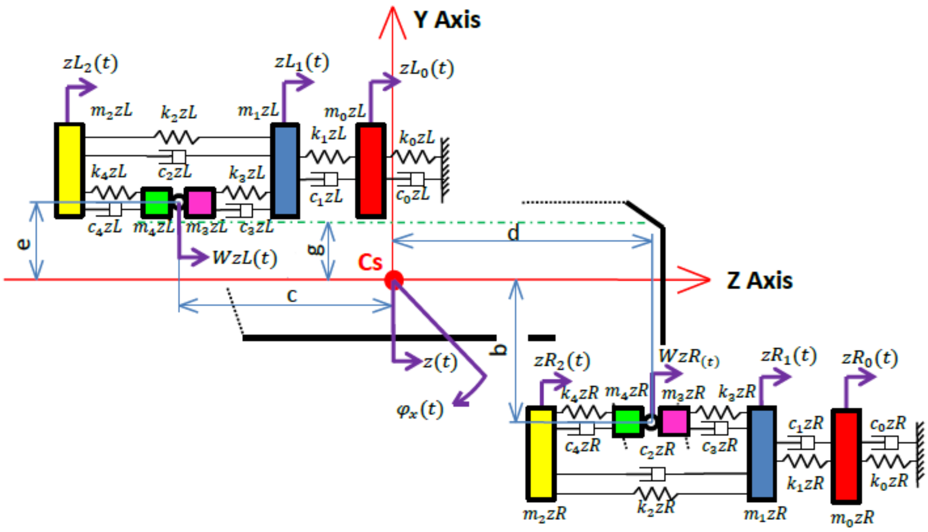

Figure 3. Equivalent model for Z direction

In the figure following markings have been adopted:
m_0zL, m_1zL, m_2zL, m_3zL, m_4zL – equivalent mass coefficients of the left hand in Z direction,
m_0zR, m_1zR, m_2zR, m_3zR, m_4zR – equivalent mass coefficients of the right hand in Z direction,
k_0zL, k_1zL, k_2zL, k_3zL, k_4zL – equivalent stiffness coefficients of the left hand in Z direction,
k_0zR, k_1zR, k_2zR, k_3zR, k_4zR – equivalent stiffness coefficients of the right hand in Z direction,
c_0zL, c_1zL, c_2zL, c_3zL, c_4zL – equivalent dumping coefficients of the left hand in Z direction,
c_0zR, c_1zR, c_2zR, c_3zR, c_4zR – equivalent dumping coefficients of the right hand in Z direction,
z(t) – linear displacement of centre of the mass in Z direction,
$\varphi_x(t)$ – angular displacement of the model around the X axis,
WzL(t) – net displacement of the device's left handle in Z direction,
WzR(t) – net displacement of the device's right handle in Z direction,
b c, d ,e, g – dimensions describing position (distance) between device's handles, spindle and the centre of the mass of the device.

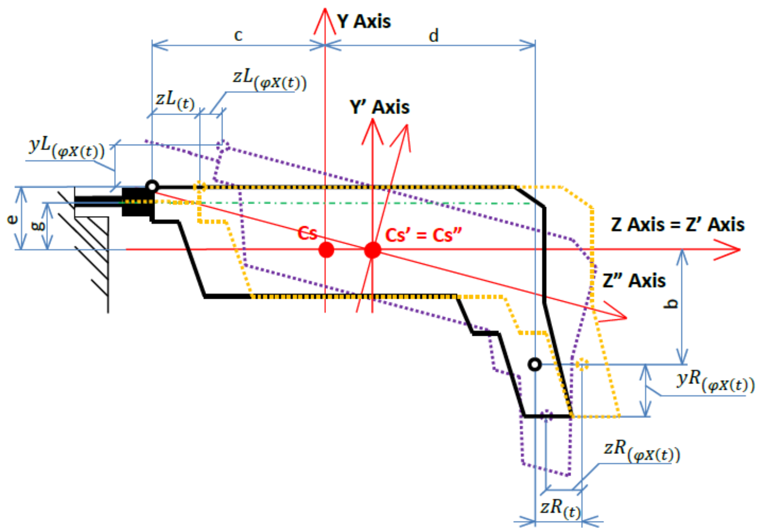

Figure 4. Displacement graph for Z direction

In the figure following markings have been adopted:

b c, d ,e, g – dimensions describing position (distance) between device's handles, spindle and the centre of the mass of the device,

zL(t) – displacement of the device's left handle in Z direction caused by linear displacement z(t),

$zL_{(\varphi x(t))}$ – displacement of the device's left handle in Z direction caused by angular displacement $\varphi_x(t)$,

$yL_{(\varphi x(t))}$ – displacement of the device's left handle in Y direction caused by angular displacement $\varphi_x(t)$,

zR(t) – displacement of the device's right handle in Z direction caused by linear displacement z(t),

$zR_{(\varphi x(t))}$ – displacement of the device's right handle in Z direction caused by angular displacement $\varphi_x(t)$,

$yR_{(\varphi x(t))}$ – displacement of the device's right handle in Y direction caused by linear displacement z(t).

Designation of parameters in the four following figures was done in accordance to designation of parameters in Figures 3 and 4.

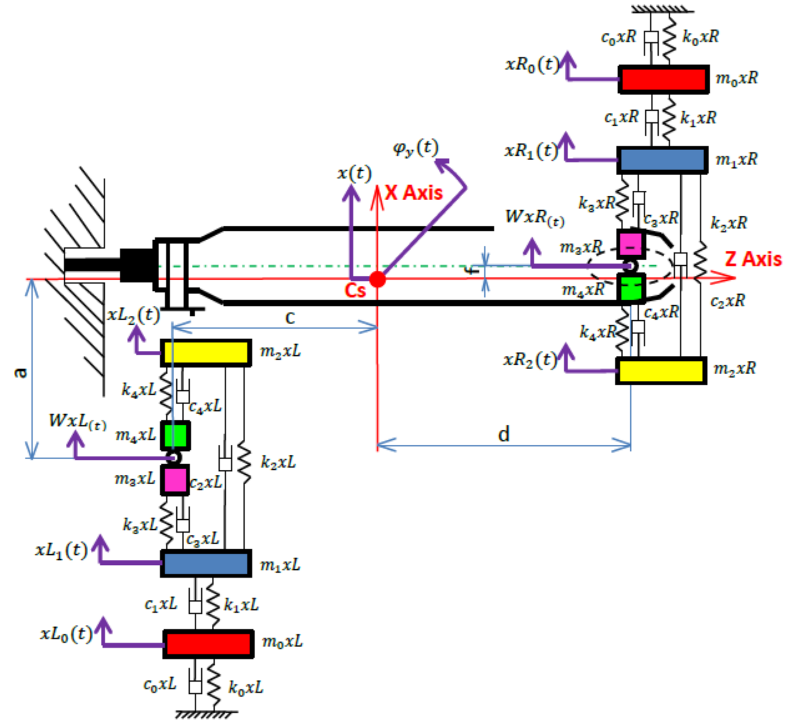

Figure 5. Equivalent model for X direction

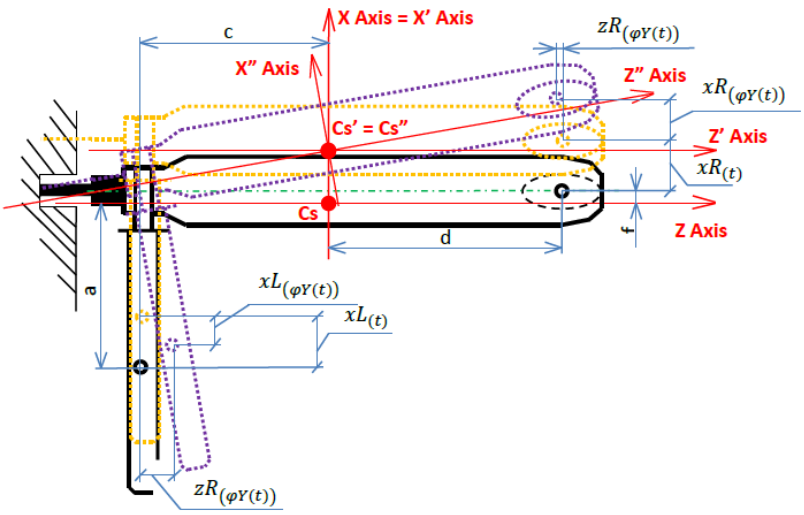

Figure 6. Displacement graph for X direction

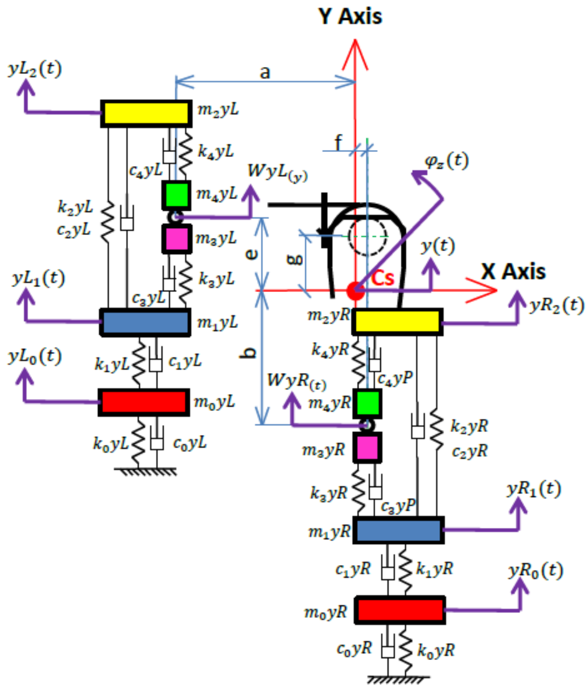

Figure 7. Equivalent model for Y direction

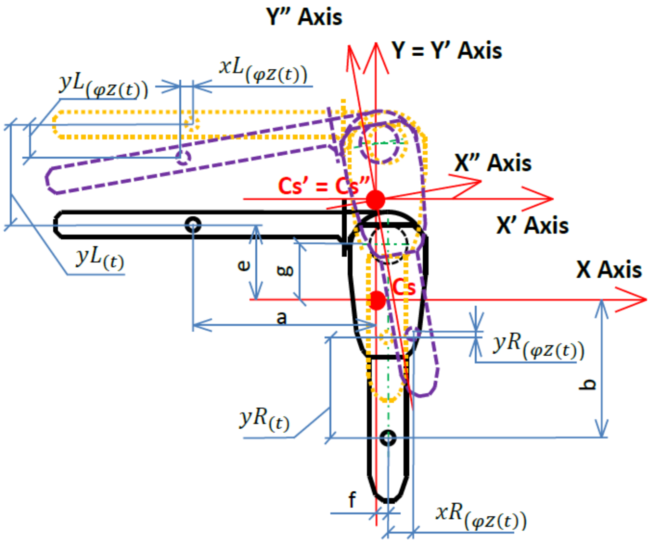

Figure 8. Displacement graph for Y direction

In order to solve the simulation model, it is necessary to determine the value of the force vector – components of the eigenvector and the eigenmoment. The determination of these values requires carrying out kinematic analyses of the device's drive. To do this, one have to define positions of all bearing nodes in relation to the device's centre of the mass. Furthermore, values of technological forces from the tool (friction strength, resistance torque, etc.) should be determined. Then basing on the knowledge of the drive structure and dimensions of its components values of reaction forces (bearings) are calculated. An assembly drawing of the analysed device with highlighted movable parts is shown in Figure 9.

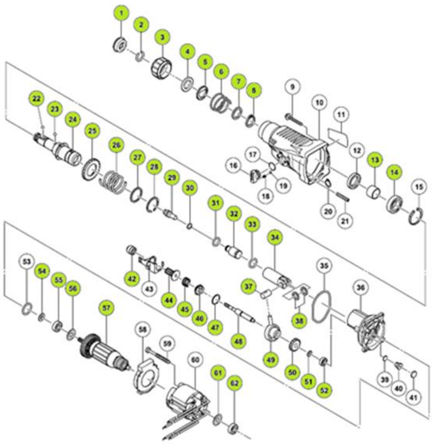

Figure 9. Assembly drawing Hitachi DH 22 PH [47]

The kinematic scheme of the driving mechanism was created based on the assembly drawing. It is presented in the following figure.

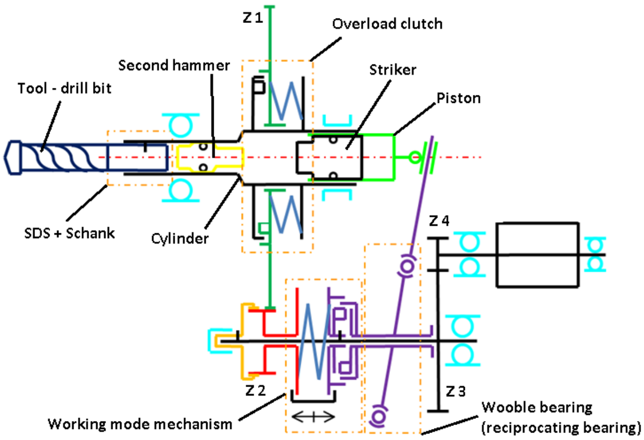

Figure 10. Kinematic scheme of the driving mechanism

The list of movable parts together with the kinematic scheme allows us to analytically determine the value of the mass moment of inertia of the driving mechanism reduced to the spindle axis - $I_Z^{\text{INT. MECH}}$.. It is described by the following equation

$$I_Z{}^{INT.MECH.} = \begin{bmatrix} (I_1 + I_2 + \cdots . + I_7 + I_8 + I_{13} + I_{14} + I_{22} + \cdots . + I_{28}) \\ + (I_{42} + I_{44} + \ldots . + I_{52}) \dfrac{Z1}{Z2} + (I_{54} + \ldots . + I_{57} + I_{61} + I_{62}) \dfrac{Z1}{Z2}\dfrac{Z3}{Z4} \end{bmatrix}$$

where: I_i – value of individual moment of inertia; *Z*1, *Z*2, *Z*3, *Z*4 – number of teeth of each gear

A force field acting on bearing nodes was also created on the basis of the kinematic scheme. The input parameters for such calculations are: technological forces, ratios of gear stages as well as geometrical dimensions of elements and arrangement of the bearings. According to reverse engineering values and frequencies of reaction forces can be calculated. These forces are transferred through the device’s body onto its handles. They form three-dimensional general force system, that according to principals of the vector calculus, reduces to the eigenvector and the eigenmoment of the entire system. The force field is shown in the figure below.

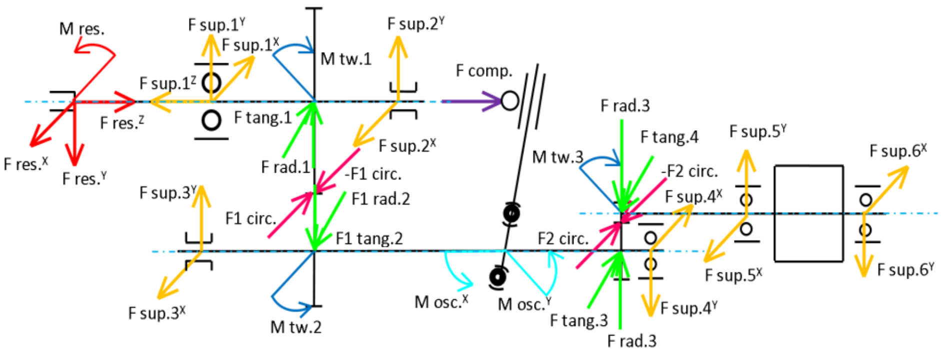

Figure 11. Drive mechanism load diagram

where: M $_{\text{res.}}$ – resistance torque; F $_{\text{res.}}{}^{i}$ – resistance force; F $_{\text{sup.}}$j ^{i} – supporting force; M $_{\text{tw. j}}$ – twisting torque; F $_{\text{comp.}}$ – compression force; F $_{\text{j circ.}}$ – circumferential force; F $_{\text{tang. j}}$ – tangential force; F $_{\text{rad. j}}$ – radial force; M $_{\text{osc.}}{}^{i}$ – oscillating moment; i – X, Y and Z - axis of coordinate system; j – index calculations – number of bearing node and stage of gear of the drive mechanism.

3. Analytical research results

The net displacement of a handle in the considered direction are a geometric sum of the linear displacement of the centre of the mass in this direction and angular displacements resulting from the rotational movement of the device relative to the other two axes of the coordinate system passing through the centre of the mass, for a specific arm measured between the centre of the mass and the reference point assigned to a the handle. The net vibrations are described for each of directions of the coordinate system, in the case of the rear handle with equations (2), (3) and (4), and for the front handle with equations (5), (6) and (7). In these equations, the net displacements of the handle – reference point, were defined as the geometric sum of the linear displacement of the device's centre of the mass and the displacement of the handle caused by rotational movement relative to axes passing through the centre of the mass. Finally, assuming the linear and angular displacements are finitely small, the components of lower orders, that are associated with to the double product of angular displacements, were omitted and resulted with the following set of equations.

$$\begin{gathered} W_R Z_{(t)} = z_{(t)} + zR_{(\varphi X(t))} + zR_{(\varphi Y(t))} \\ = z_{(t)} + \left(-b \cdot \varphi_{x(t)} - d \cdot \varphi_{x(t)} \cdot \varphi_{x(t)}\right) + \left(-f \cdot \varphi_{y(t)} - d \cdot \varphi_{y(t)} \cdot \varphi_{y(t)}\right) \\ \cong z_{(t)} - b \cdot \varphi_{x(t)} + f \cdot \varphi_{y(t)} \end{gathered} \tag{2}$$

$$\begin{gathered} W_R X_{(t)} = x_{(t)} + xR_{(\varphi Y(t))} + xR_{(\varphi Z(t))} \\ = x_{(t)} + \left(d \cdot \varphi_{y(t)} + d \cdot \varphi_{y(t)} \cdot \varphi_{y(t)}\right) + \left(-f \cdot \varphi_{y(t)} - d \cdot \varphi_{y(t)} \cdot \varphi_{y(t)}\right) \\ \cong x_{(t)} - d \cdot \varphi_{y(t)} + f \cdot \varphi_{y(t)} \end{gathered} \tag{3}$$

$$\begin{gathered} W_R Y_{(t)} = y_{(t)} + yR_{(\varphi X(t))} + yR_{(\varphi Z(t))} \\ = y_{(t)} + \left(-d \cdot \varphi_{x(t)} + b \cdot \varphi_{x(t)} \cdot \varphi_{x(t)}\right) + \left(f \cdot \varphi_{z(t)} + b \cdot \varphi_{z(t)} \cdot \varphi_{z(t)}\right) \\ \cong y_{(t)} - d \cdot \varphi_{x(t)} + f \cdot \varphi_{z(t)} \end{gathered} \tag{4}$$

$$\begin{gathered} W_L Z_{(t)} = z_{(t)} + zL_{(\varphi X(t))} + zL_{(\varphi Y(t))} \\ = z_{(t)} + \left(e \cdot \varphi_{x(t)} + c \cdot \varphi_{x(t)} \cdot \varphi_{x(t)}\right) + \left(a \cdot \varphi_{y(t)} + c \cdot \varphi_{y(t)} \cdot \varphi_{y(t)}\right) \\ \cong z_{(t)} + e \cdot \varphi_{x(t)} + a \cdot \varphi_{y(t)} \end{gathered} \tag{5}$$

$$\begin{gathered} W_L X_{(t)} = x_{(t)} + xL_{(\varphi Y(y))} + xL_{(\varphi Z(t))} \\ = x_{(t)} + \left(-c \cdot \varphi_{y(t)} + a \cdot \varphi_{y(t)} \cdot \varphi_{y(t)}\right) + \left(-e \cdot \varphi_{z(t)} + a \cdot \varphi_{z(t)} \cdot \varphi_{z(t)}\right) \\ \cong x_{(t)} - c \cdot \varphi_{y(t)} - e \cdot \varphi_{z(t)} \end{gathered} \tag{6}$$

$$\begin{gathered} W_L Y_{(t)} = y_{(t)} + yL_{(\varphi X(t))} + yL_{(\varphi Z(t))} \\ = y_{(t)} + \left(c \cdot \varphi_{x(t)} - e \cdot \varphi_{x(t)} \cdot \varphi_{x(t)}\right) + \left(-a \cdot \varphi_{z(t)} - e \cdot \varphi_{z(t)} \cdot \varphi_{z(t)}\right) \\ \cong y_{(t)} - c \cdot \varphi_{x(t)} - a \cdot \varphi_{z(t)} \end{gathered} \tag{7}$$

The mathematical model of the analysed bio-mechanical system was developed using the Lagrange's equations of the second kind. For each of the reference points, directions of vibration and type of motion device (linear and angular), the motion equation was derived individually. The general form of the Lagrange's equation is presented by equation (8).

$$\frac{d}{dt}\left(\frac{\partial E_K}{\partial \dot{q}_j}\right) - \frac{\partial E_K}{\partial q_j} = \frac{\partial L}{\partial q_j} - \frac{\partial V}{\partial q_j} - \frac{\partial \emptyset}{\partial \dot{q}_j} \tag{8}$$

where: E_K – total kinetic energy of the reduction point; L- virtual work of stimulating force at the point of reduction; V-potential elastic forces; Ø –power dissipation function; q- generalized coordinate; j – index calculations; j = 1,2, 3, …, s; s – number of degrees of freedom

Determination of the net accelerations requires knowledge of the values of linear displacements and rotational movements performed in relation to the axes passing through the device's centre of the mass. This leads to formulation and solution (numerically) of the mathematical model - 24 differential motion equations, which representation can be shortened by using the matrix notation and equation (1). Then the general form of the components of this equation is given in the following form:

A) Displacement vector and inertia matrix:

$$q_{(t)} = \begin{bmatrix} iR_{0(t)} \\ iL_{0(t)} \\ iR_{1(t)} \\ iL_{1(t)} \\ iR_{2(t)} \\ iL_{2(t)} \\ i_{(t)} \\ \varphi_{i(t)} \end{bmatrix} \qquad [M] = \begin{bmatrix} m_{0iR} & 0 & 0 & 0 & 0 & 0 & 0 & 0 \\ 0 & m_{0iL} & 0 & 0 & 0 & 0 & 0 & 0 \\ 0 & 0 & m_{1iR} & 0 & 0 & 0 & 0 & 0 \\ 0 & 0 & 0 & m_{1iL} & 0 & 0 & 0 & 0 \\ 0 & 0 & 0 & 0 & m_{2iR} & 0 & 0 & 0 \\ 0 & 0 & 0 & 0 & 0 & m_{2iL} & 0 & 0 \\ 0 & 0 & 0 & 0 & 0 & 0 & M_i & 0 \\ 0 & 0 & 0 & 0 & 0 & 0 & 0 & J_i^{RED.} \end{bmatrix}$$

B) Dumping matrix:

$$[C] = \begin{bmatrix} c_{0iR}+c_{1iR} & 0 & -c_{1iR} & 0 & 0 & 0 & 0 & 0 \\ 0 & c_{0iL}+c_{1iL} & 0 & -c_{1iL} & 0 & 0 & 0 & 0 \\ -c_{1iR} & 0 & c_{1iR}+c_{2iR}+c_{3iR} & 0 & -c_{2iR} & 0 & -c_{3iR} & 0 \\ 0 & -c_{1iL} & 0 & c_{1iL}+c_{2iL}+c_{3iL} & 0 & -c_{2iL} & -c_{3iL} & 0 \\ 0 & 0 & -c_{2iR} & 0 & c_{2iR}+c_{4iR} & 0 & -c_{4iR} & 0 \\ 0 & 0 & 0 & -c_{2iL} & 0 & c_{2iL}+c_{4iR} & -c_{4iL} & 0 \\ 0 & 0 & -c_{3iR} & -c_{3iL} & -c_{4iR} & -c_{4iL} & C_iZ & 0 \\ 0 & 0 & 0 & 0 & 0 & 0 & 0 & C_i\varphi \end{bmatrix}$$

C) Stiffness matrix:

$$[K] = \begin{bmatrix} k_{0iR}+k_{1iR} & 0 & -k_{1iR} & 0 & 0 & 0 & 0 & 0 \\ 0 & k_{0iL}+k_{1iL} & 0 & -k_{1iL} & 0 & 0 & 0 & 0 \\ -k_{1iR} & 0 & k_{1iR}+k_{2iR}+k_{3iR} & 0 & -k_{2iR} & 0 & -k_{3iR} & 0 \\ 0 & -k_{1iL} & 0 & k_{1iL}+k_{2iL}+k_{3iL} & 0 & -k_{2iL} & -k_{3iL} & 0 \\ 0 & 0 & -k_{2iR} & 0 & k_{2iR}+k_{4iR} & 0 & -k_{4iR} & 0 \\ 0 & 0 & 0 & -k_{2iL} & 0 & k_{2iL}+k_{4iR} & -k_{4iL} & 0 \\ 0 & 0 & -k_{3iR} & -k_{3iL} & -k_{4iR} & -k_{4iL} & K_iZ & 0 \\ 0 & 0 & 0 & 0 & 0 & 0 & 0 & K_i\varphi \end{bmatrix}$$

where: i = X, Y, Z - direction of the coordinate system.

The displacement vector is the effect of double integration of the acceleration vector of each of reference points. Currently, for this purpose, numerical integration procedures

(ODE 113 and others) implemented in a digital simulation software are used, e.g. Matlab SIMULINK.

In the above matrices in addition to the individual (or in the form of appropriate algebraic expressions) mass, stiffness and damping parameters, whose values were specified in ISO 10068, there are also generalized equivalent coefficients of mass, stiffness and damping. In the case when the Z direction is considered, the generalized equivalent parameters are:

A) Generalized equivalent mass coefficient

$$M_Z = M_D + m_{3ZR} + m_{4ZR} + m_{3ZL} + m_{4ZL} \tag{9}$$

where: M_D – the device's mass

B) Generalized equivalent moment of inertia

$$J_Z{}^{RED.} = \begin{bmatrix} J_Z{}^{INT.\ MECH.} + (m_{3XR} + m_{4XR})b^2 + (m_{3XL} + m_{4XL})e^2 \\ +(m_{3YR} + m_{4YR})f^2 + (m_{3YL} + m_{4YL})a^2 \end{bmatrix} \tag{10}$$

where: $I_Z{}^{INT.MECH.}$ – moment of inertia of the drive mechanism generalized to the spindle axis.

C) Generalized equivalent damping coefficient for translations

$$C_Z Z = c_{3ZR} + c_{4ZR} + c_{3ZL} + c_{4ZL} \tag{11}$$

D) Generalized equivalent damping coefficient for rotations

$$C_Z \varphi = [(c_{3XR} + c_{4XR})b^2 + (c_{3XL} + c_{4XL})e^2 + (c_{3YR} + c_{4YR})f^2 + (c_{3YL} + c_{4YL})a^2] \tag{12}$$

E) Generalized equivalent stiffness coefficient for translations

$$K_Z Z = k_{3ZR} + k_{4ZR} + k_{3ZL} + k_{4ZL} \tag{13}$$

F) Generalized equivalent stiffness coefficient for rotations

$$K_Z \varphi = [(k_{3XR} + k_{4XR})b^2 + (k_{3XL} + k_{4XL})e^2 + (k_{3YR} + k_{4YR})f^2 + (k_{3YL} + k_{4YL})a^2] \tag{14}$$

For the other two coordinate system axes, in equations describing the values of equivalent dynamic parameters, in addition to the change of the index of a given axis (for coefficients associated with translations), the dimensions are switched for the corresponding to position related to the given axis - in the case of parameters related to rotational motion.

5. Preliminary simulation results

The results of a simplified simulation concerning only translation in the Z axis are presented below. It was assumed that the motion is the result of the simultaneous operation of a sinusoidal pressure force and the impulse force associated with the impact mechanism

Simulation parameters: mass, stiffness and dumping coefficients in the direction of the spindle axis - Z axis were adopted in accordance with ISO 10068. The mass of the device equals 2.1 kg, while the source of vibration was represented in the form of a sinusoidal signal with an amplitude of 90 N and a frequency of 23.3 Hz. Then, the impact mechanism was modelled as impulses with an amplitude of 270 μm, duration of 0.01 s and 1% signal fill time. Zero initial conditions were also assumed. The system began its motion from rest. Due to the symmetry of the system: both in terms of physical structure and parameter values (coefficients), vibrations of individual reference points for both limbs are the same. In addition, handle vibrations are equal to the vibrations of the device's centre of the mass.

The *RMS* values of acceleration, velocity and displacement of the reference points are presented in the table 1.

Table 1. RMS value of dynamic simulation parameter

	Dynamic parameter		
Point of reduction	Acceleration	Velocity	Displacement
	[m/s^2]	[m/s]	[m]
z(t) = zP(t) = zL(t)	12.61	0.09426	0.004019
zP2(t) = zL2(t)	4.67	0.08931	0.003808
zP1(t) = zL1(t)	2.342	0.09609	0.004099
zP0(t) = zL0(t)	0.9721	0.04104	0.001747

The simulation results in the form of acceleration, velocity and displacement signals of individual reference points are presented below. Firstly, the results related to reference points associated with the handles of the device were presented, these are followed by the results for points related to the masses m_2, m_1 and m_0.

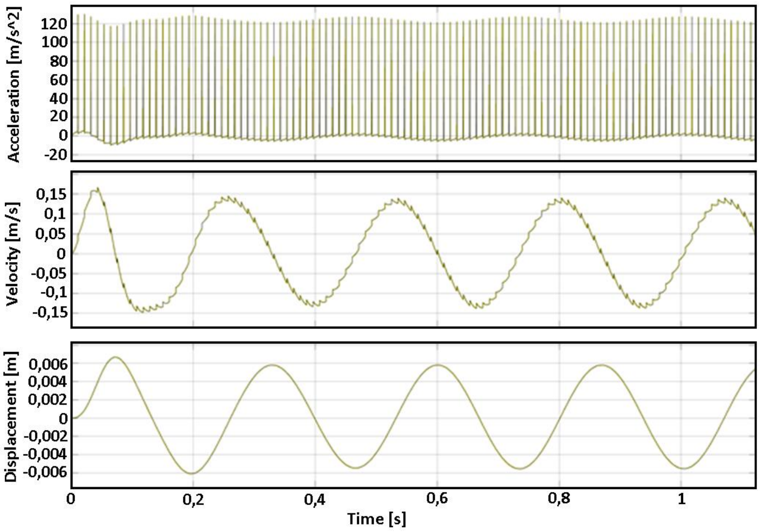

Figure 12. Accelerations, velocity and displacement of the handle – mass m_3 and m_4

As shown in Figure 12, the peak values of vibration acceleration of both the reference points fixed to the device's handles exceed 120 m/s^2. Accelerations are sinusoidal with a few impulse events. Numerical integration, through which velocities and displacements are calculated, decreases the impact character of the operation. The peak values of velocity reach approx. 0.15 m/s, while peak values of displacement are approx. equal to 7 mm. The transient state associated with the start-up phase lasts approx. 0.5 seconds.

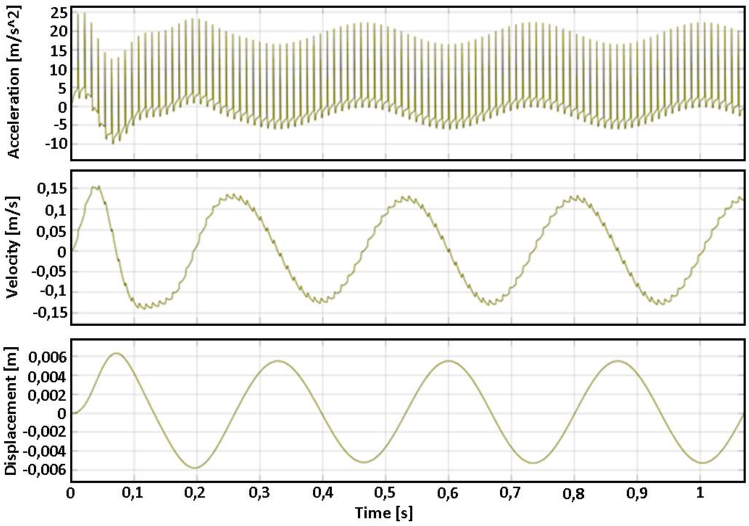

Figure 13. Accelerations, velocity and displacement of the m_2 mass point reduction

Vibration accelerations of the reference point corresponding to the movement of mass m_2 reach a value of about 23 m/s^2, the peak values of vibration velocity, likewise for the handle of the device, are approx. equal to 0.15 m/s. Peak values of displacements are slightly smaller than for the handle and are approx. equal to 6 mm. The nature of the time course of dynamic parameters is similar to one for the before mentioned reference point. For mass m_2, the impulse character of the vibrations also disappears with each subsequent signal integration.

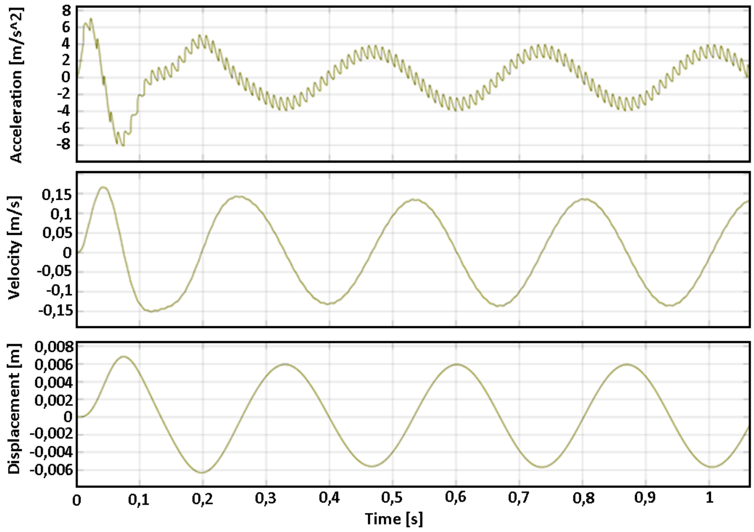

Figure 14. Accelerations, velocity and displacement of the m_1 mass point reduction

As it is shown in Figure 14 for the reference point associated with mass m_1, the peak value of vibration acceleration is about 4 m/s^2. The peak value of vibration velocity, as in previous cases, is approx. equal to 0.15 m/s. Furthermore, the amplitudes of vibration displacements are about 6 mm. In the case of vibration accelerations for mass m_1, no phenomena related to the impact mechanism have been observed. The same it was for previously considered reference points.

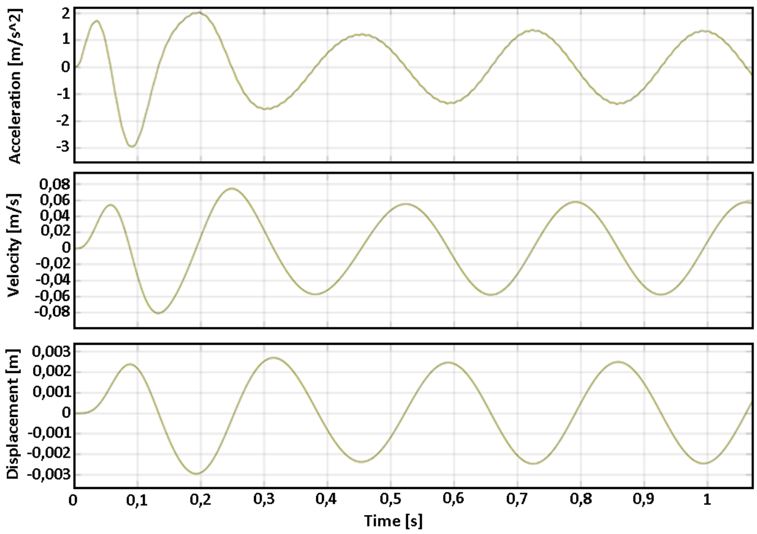

Figure 15 Accelerations, velocity and displacement of the m_0 mass point reduction

For the reference point representing mass movement m_0, the peak values of vibration acceleration shown in the figure do not exceed 1.2 m/s^2. The peak value of vibration velocity equals 0.06 m/s, while the peak vibration displacements are about 2.5 mm. The visible start-up phase, as well as for the previously analysed reference points, lasts about 0.5 seconds.

6. Conclusions

Using the Lagrange's equations of the second kind, it is possible to build a mathematical model describing the vibrations of any mechanical and/or bio-mechanical system.

The ISO 10068 standard provides 3 variants of the upper limb model. For the purposes of the research, the five degrees of freedom (5 dof) equivalent model of upper limb was used.

The development of the mathematical model requires determining the distance between the device's centre of the mass and it's handles as well as calculating moments of inertia in relation to the coordinate system axes.

The structural analysis of the drive mechanism allows us to determine the values of forces acting on individual bearing nodes. Using the theorem on the reduction of any spatial system of forces, one can determine the values of the eigenvector and the eigenmoment of the system in relation to the centre of the mass of the system.

The solution of the mathematical model requires the use of simulation software and a numerical integration apparatus. It is necessary to know the nature and the actual value of the stimulating forces acting on the system.

The determination of values of the mass moments of inertia of the device's drive, regardless from its type and size, requires running structural and kinematic analysis. For this purpose, one can use tools commonly used in engineering practice, e.g. CAx programs such as Matlab SIMULINK. In the case of the lack of digital documentation of a device, it is necessary to disassemble the device and to map the geometry and kinematic structures of the drive system elements.

The ISO 10068 standard allows an approximate determination of the dynamic parameters of individual parts of the upper limbs when the nature of the source of vibration is known. It is possible without interfering with the operator's body.

On the basis of the results of simulations, it was found that the vibrations emitted by the device exceed both the threshold limit value for an 8-hour working day and for short-term exposure, which has been confirmed in stand tests [45].

Following the path of reference points from the device - the consecutive reference points, the vibration load of individual parts of the operator's upper limbs decreases. At the same time, the phenomena related to the impulse nature of the device's operation disappear.

The simulation model provides the opportunity to analyse transient states by setting elective initial parameter values.

Acknowledgement

This paper was financially supported in the year 2019 by research project 02/21/SBAD/3558/2019.

References

1. P. Paczos, R. Wichniarek, K. Magnucki, *Three–point bending of sandwich beam with special structure of the core*, Composite Structures, **201** (2018) 676 – 682.
2. M. Obst, D. Kurpisz, P. Paczos, *The experimental and analitical investigations of torsion phenomenon of thin–walled cold formed channel beams subjected to four–point bending*, Thinn–Walled Structures, **106** (2016) 179 – 186.
3. P. Paczos, P. Wasilewicz, E. Magnucka–Blandzi, *Experimental and numerical investigations of five–layered trapezoidal beams*, Composite Structures, **145** (2016) 129 – 141.
4. M. Obst, M. Rodak, P. Paczos, *Limit load of cold formed thin–walled nonstandards channel beams*, Journal of Theoretical and Applied Mechanics, **54**(4) (2016) 1369 – 1377.
5. E. Magnucka–Blandzi, P. Paczos, P. Wasilewicz, A. Wypych, *Three–point bending of seven layers beams – theoretical and experimental studies*, Archives of Civil Engineering, **62**(2) (2016) 115 – 133.
6. P. Paczos, *Experimental investigations of C–beams with non–standard flanges*, Journal of Constructional Steel Research, **93** (2014) 77 – 87.
7. F. Harmit , B. Necib, *Analysis of mechanical structures using plate finite element method under different boundary conditions*, Diagnostyka, **19**(2) (2018) 3 – 9.
8. J. Blata, D. Šeděnka, L. Kašiar, P. Volna, *Examining the condition of the ball and the ball track on the heavy machine ZP6600*, Diagnostyka, **18**(3) (2017) 85 – 91.

9. Y. Basova, K. Nutsubidze, M. Ivanova, S. Slipchenko, A. Kotliar, *Design and numerical simulation of the new design of the gripper for manipulating of the rotational parts*, Diagnostyka, **19**(4) (2018) 11 – 18.
10. A. Wang, J. Wang, *Temperature Distribution and Scuffing of Tapered Roller Bearing*, Chinese Journal of Mechanical Engineering, **27**(6) (2014) 1272 – 1279.
11. K. Yan, N. Wang, Q. Zhai, Y. Zhu, J. Zhang, Q. Niu, *Theoretical and experimental investigation on the thermal characteristics of double–row tapered roller bearings of high speed locomotive*, International Journal of Heat and Mass Transfer, **84** (2015) 1119 – 1130.
12. J. Li, J. Xue, Z. Ma, *Study on the Thermal Distribution Characteristics of High–Speed and Light–Load Rolling Bearing Considering Skidding*, Applied Sciences, **1593**(8) (2018) 1 – 20.
13. H. Nourghassemi, H. Ghassemi, H. Taghva, *Numerical Hydrodynamic Results of the Two Stedded Planing Hull*, American Journal of Mechanical Engineering, **6**(3) (2018) 93 – 97.
14. S. Boulahrouz, Y. Avenas, A. Chehhat, *CFD Simulation of Heat Transfer and Fluid Flow within Metalic Foam in Forced Convection Environment*, Mechanics and Mechanical Engineering, **21**(3) (2017) 611 – 635.
15. S. Bigham, H. Shokouhmand, R. N. Isfahani, S. Yazdani, *Fluid Flow and Heat Transfer Simulation in a Constricted Microchannel: Effects of Rarefaction, Geometry, and Viscous Dissipation*, Numerical Heat Transfer Applications, **59**(3) (2011) 209 – 230.
16. V. Dmytriv, I. Dmytriv, I. Horodetskyy, T. Dmytriv, *Analytical dynamic model of coefficient of friction of air pipeline under pressure*, Diagnostyka, **20**(4) (2019) 89 – 94.
17. J. Jiang, T. He, H. Duan, B. Li, *Electric Field Structure Analysis and Experimentation of Needle–plate Type Electrospinning Machine*, International Journal of Control and Automation, **7**(1) (2014) 369 – 378.
18. L. Chen, W. Lai, J. Wang, G. Jiang, Y. Zhou, Y. Chen, H. Liu, Z. Qin, L. Ke, L. Wang, Y. Shen, *Study on Surface Electric Field Simulation of High Voltage Transmission Line Assembly*, Journal of Power and Energy Engineering, **2** (2014) 554 – 563.
19. R. S. Ahmad, A. B. Shaari, C. T. Han, *Magnetic Field Simulation of Golay Coil*, Journal of Fundamental Science, **4** (2008) 353 – 361.
20. C. Ghnatios, F. Chinesta, A. Barasinski, *Electrical Fields Simulation in Heterogenus Domain Using the Proper Generalized Decomposition*, ECCOMAS Congress 2016, VII European Congress on Computational Methods in Applied Sciences and Engineering; June 2016.
21. C. Zhang Y. Mao, S. Xie, Y. Zhang, *Electric Field Simulation of Surge Capacitors with Typical Defects*, IOP Conference Series: Materials Science and Engineering, **322** (2018) 072040.

22. T. Li, Y. Jiang, L. Zhao, Y. Wang, *Electrical Field Simulation and Analysis of 1200 kV Gas Insulated Test Reactors*, IOP Conference Series: Earth and Environmental Science, **237** (2019) 062048.
23. H. Benguesmia, N. M'izou, A. Boubakeur, *Simulation of the potential and electric field distribution on high voltage insulator using the finite element method*, Diagnostyka, **19**(2) (2018) 41 – 52.
24. H. Benguesmia, B. Bakri, S. Khadar, F. Hamrit, N. M'izou, *Experimental study of pollution and simulation on insulators using COMSOL® under AC voltage*, Diagnostyka, **20**(3) (2019) 1 – 9.
25. B. Mânescu, N. D. Stânescu, *Dynamic Analisys of a Mechanism of an Engine with Variable Compression Ratio*, IOP Conference Series: Materials Science and Engineering, **564** (2019) 012118.
26. Z. Cao, S. Cao, X. Xu, T. Han, H. Guo, *Dynamic Analysis of the Harvester Seat*, IOP Conference Series: Materials Science and Engineering, **452** (2018) 022013.
27. C. Copilusi, N. Dumitru, A. Margine, I. Geonea, *Dynamic Analysis of a Human Ankle Joints Prothesis*, IOP Conference Series: Materials Science and Engineering, **568** (2019) 012077.
28. S. Maraş, M. Yaman, *Dynamic Analysis of Hybrid Laminated Composite Curved Beam*, 3rd International Conference on Advanced Engineering Technologies, September 2019
29. S. Maraş, M. Yaman, M. F. Şansveren, *Dynamic Analysis of Laminated Syntactic Foam Beams*, 3rd International Conference on Advanced Engineering Technologies, September 2019
30. V. M. Chau, H. B. Vo, *Structural Dynamics Analysis of 3-U Cube Sat*, Applied Mechanics and Materials, **894** (2019) 164 – 170.
31. A. Khnaijar, R. Benamar, *A discrete model for nonlinear vibrations of a simply supported cracked beams resting on elastic foundations*, Diagnostyka, **18**(3) (2017) 39 – 46.
32. M. Guebailia, N. Ouelaa, *The dynamic response of a continuous plate for different surface states*, Diagnostyka, **18**(4) (2017) 11 – 17.
33. J. Zachwieja, *Pipeline stress analysis under supporting structure vibrations*, Diagnostyka, **18**(2) (2017) 23 – 30.
34. Y. Kharchenko, Ł. Dragun, *Mathematical modelling of unsteady processes in electromechnical system of ring–ball mill*, Diagnostyka, **18**(1) (2017) 25 – 35.
35. EN ISO 5349–1 Mechanical Vibration – Measurement and Evaluation of Human Exposure to Hand-Transmitted Vibration – Part 1: General Requirements.
36. EN ISO 5349–2 Mechanical Vibration – Measurement and Evaluation of Human Exposure to Hand-Transmitted Vibration – Part 2: Practical Guidance for Measurement at the Workplace.
37. G. Bąk, E. Cukierman–Rakoczy, *Dynamic reaction of a human on vibrations by analysis of a single-dimensional biomechanical model*, Biuletyn Wojskowej Akademii Technicznej, **67** – LXVII (4) (2018) 169 – 181 (in Polish).

38. W. Mrukwa, J. Świder, A. Staniek, *Assessment of vibration measurement possibility at the contact point of hands with the vibration source*, Prace Naukowe Głównego Instytutu Górnictwa – Górnictwo i Środowisko, **1** (2002) 91 – 102.
39. A. M. Książek, *Analysis of existing biodynamic models of the hand-arm system for human vibration isolation - the operator from vibrations emitted by hand tools*, Czasopismo Techniczne 2M/1996, Wydawnictwo Politechniki Krakowskiej, 87 – 114 (in Polish).
40. M. Nader, J. Korzeb, *The Review of Biomechanical Models to Assess the Impact of Vibrations upon Human Organism*, Materials of a 3rd National Symposium "Computer – Aided Systems for Engineering Works in Industry and Transportation", 1999.
41. ISO 10068:1998 – *Mechanical vibration and shock - Free, mechanical impedance of the human hand-arm system at the driving point.*
42. M. W. Dobry, T. Hermann, *Energy method of an evaluation of human mechanical and biomechanical systems*, Modelowanie Inżynierskie, **17**(48) (2013) 28 – 36.
43. A. Antonucci, A. Barr, B. Martin, D. Rempel, *Effect of bit wear on hammer drill handle vibration and productivity*, Journal of Occupational and Environmental Hygiene, **14**(8) (2017) 641 – 649.
44. B. Jakubek, W. Rukat, *Influence of a tool's working diameter on the level of handle vibrations of an impact drill*, Vibroengineering Procedia, **6** (2015) 288 – 291.
45. B. Jakubek, W. Rukat, *Comparison of vibration impact of an impact drill on the human body under different working conditions*, Vibrations in Physical Systems, **27** (2017) 135 – 142.
46. Handling instruction for Hitachi DH 22PH rotary hammer – Code No. C99179291 F; downloaded from the site: https://hikoki-narzedzia.pl/do_pobrania; Access date: 5 II 2020.